Ab initio investigations of the electronic structure and chemical bonding of Li_2ZrN_2

S.F. Matar [a,*], R. Pöttgen [b], A.F. Al Alam [c], N. Ouaini [c]

[a] CNRS, Université de Bordeaux, ICMCB, 87 Avenue du Docteur Albert Schweitzer, 33600 Pessac, France
[b] Institut für Anorganische und Analytische Chemie, Universität Münster, Corrensstrasse 30, D-48149 Münster, Germany
[c] Université Saint Esprit de Kaslik (USEK), Faculté des Sciences, URA GREVE (CNRS/USEK/UL), Jounieh, Lebanon

ARTICLE INFO

ABSTRACT

The electronic structure of the ternary nitride Li_2ZrN_2 is examined from ab initio with DFT computations for an assessment of the properties of chemical bonding. The compound is found insulating with 1.8 eV band gap; it becomes metallic and less ionic upon removal of one equivalent of Li. The chemical interaction is found mainly between Zr and N on one hand and Li and N on the other hand. While all pair interactions are bonding, antibonding N–N interactions are found dominant at the top of the valence band of Li_2ZrN_2 and they become less intense upon removal of Li. From energy differences the partial delithiation leading to $Li_{2-x}ZrN_2$ ($x = \sim 1$) is favored.

© 2012 Elsevier Inc. All rights reserved.

1. Introduction

In recent decades several classes of non-oxide lithium compounds were investigated for their use as negative electrode materials in lithium-ion batteries [1,2]. Besides silicides [3,4], sulfides [5,6] and phosphides [6], lithium transition metal nitrides [6,7] were examined as promising anode material. Along with the many phase analytical and electrochemical studies of such materials, comparatively few investigations focused on the electronic structure and chemical bonding, e.g. for $Li_{15}Si_4$ [8] or Li_xFeS_2 [9].

In the course of our systematic studies of structure–property relationships and chemical bonding of binary and ternary lithium-based silicides ([4,10–16], and references therein) we recently investigated the electron precise silicides YLiSi ($\equiv Y^{3+}Li^+Si^{4-}$) [16] and $La_2Li_2Si_3$ ($\equiv 2La^{3+}2Li^+2Si1^{2-}Si2^{4-}$) [15]. Such materials are potential candidates when searching for lithium mobility. Indeed, the calculations for YLiSi [16] indicated the possibility of an at least partial delithiation $Li_{1-x}YSi$, while keeping the yttrium–silicon substructure. Extending this work we were interested in the bonding patterns of related lithium nitridometalates $Li_x[T_yN_z]$. Out of the huge number of lithium

nitridometalates [17–22] we choose the structure of Li_2ZrN_2 [23,24]. This nitridometalate was first synthesized by Palisaar and Juza in 1971 from a reaction between lithium nitride Li_3N and nitrogen excess $ZrN_{1.22}$ in an ammonia flow at high temperature [23]. The structure was determined by powder X-ray diffraction without further characterization of its physical properties. Later on, Niewa and Jacobs reinvestigated Li_2ZrN_2 by neutron powder diffraction [24]. They fully confirmed the original structural model, however, with better precision, especially for the weakly scattering (X-rays) lithium atoms.

Li_2ZrN_2 has been studied with respect to the electrical conductivity, by solid state NMR spectroscopy [25], and coulometric titration [26], indicating that this nitridometalate might be suitable for high-temperature lithium batteries. Keeping these favorable properties in mind we studied the electronic structure and the properties of chemical bonding and potential delithiation of Li_2ZrN_2 within the quantum theoretical framework of the density functional theory (DFT) [27,28].

2. Computational methodology

Two computational methods within the DFT were used in a complementary manner. The Vienna ab initio simulation package (VASP) code [29,30] allows geometry optimization and total energy calculations. For this we use the projector augmented wave (PAW) method [30,31], built within the generalized gradient approximation (GGA) scheme following Perdew, Burke and

* Corresponding author. Fax: +33 5 4000 2761.
E-mail addresses: matar@icmcb-bordeaux.cnrs.fr (S.F. Matar),
pottgen@uni-muenster.de (R. Pöttgen), adelalalam@usek.edu.lb (A.F. Al Alam),
naimouaini@usek.edu.lb (N. Ouaini).

Ernzerhof (PBE) [32]. The conjugate-gradient algorithm [33] is used in this computational scheme to relax the atoms. The tetrahedron method with Blöchl corrections [31] as well as a Methfessel-Paxton [34] scheme were applied for both geometry relaxation and total energy calculations. Brillouin-zone (BZ) integrals were approximated using the special k-point sampling of Monkhorst and Pack [35]. The optimization of the structural parameters was performed until the forces on the atoms were less than 0.02 eV/Å and all stress components less than 0.003 eV/Å^3. The calculations are converged at an energy cut-off of 400 eV for the plane-wave basis set with respect to the k-point integration with a starting mesh of $4 \times 4 \times 4$ up to $8 \times 8 \times 8$ for best convergence and relaxation to zero strains.

Then all-electron calculations, equally based on the DFT with the GGA-PBE functional [32], were carried out for a full description of the electronic structure and the properties of chemical bonding. They were performed using the full potential scalar-relativistic augmented spherical wave (ASW) method [36,37]. In the ASW method, the wave function is expanded in atom-centered augmented spherical waves, which are Hankel functions and numerical solutions of Schrödinger's equation, respectively, outside and inside the so-called augmentation spheres. In the minimal ASW basis set, we chose the outermost shells to represent the valence states and the matrix elements were constructed using partial waves up to $l_{max}+1=3$ for Zr and $l_{max}+1=2$ for Li and N. Self-consistency was achieved when charge transfers and energy changes between two successive cycles were below 10^{-8} and 10^{-6} eV, respectively. The Brillouin zone integrations were performed using the linear tetrahedron method within the irreducible wedge [31]. The calculations are carried out assuming spin degenerate configuration. Besides the site projected density of states, we discuss qualitatively the pair interactions based on the overlap population analysis with the crystal orbital overlap population (COOP) [38]. In the plots, positive, negative, and zero COOP magnitudes indicate bonding, antibonding, and non-bonding interactions, respectively. We note that another scheme for describing the chemical bonding, the ECOV (covalent bond energy) criterion based on both the overlap and the Hamiltonian populations is also accessible within the ASW method [37]. It provides similar qualitative results to the COOP.

3. Crystal structure

The trigonal structure (Table 1) of Li_2ZrN_2 [23,24] is sketched in Fig. 1. Along the c-axis it consists of a succession of Zr–N–Li layers, with Li tetrahedrally coordinated to N while Zr is found in an octahedral nitrogen environment. The shortest interatomic distances occur for Li–N (2.098 Å) and Zr–N (2.253 Å), compatible with the sum of the covalent radii of 1.93 Å and 2.15 Å ($r_{Li}=1.23$ Å, $r_{Zr}=1.45$ Å and $r_N=0.70$ Å). Thus significant bonding can be expected for Li–N and Zr–N in the ternary nitride. This is explained further in next sections.

4. Results of geometry optimizations, energies and electron localization

Geometry optimization was carried out for Li_2ZrN_2 starting with the literature data [24]. Table 1 provides the experimental and calculated crystal structure characteristics. The geometry optimized lattice parameters and atomic positions are found in fairly good agreement with the experimental X-ray [23] and neutron powder determination data [24], especially for the internal coordinates of N and Li. In order to examine the effect of lithium de-intercalation, two additional calculations were done assuming a departure of one out of the two lithium atoms leading to the composition "$LiZrN_2$" and a hypothetic lithium-free compound "ZrN_2". The results are given in 3rd and 4th columns of Table 1.

The full geometry relaxation keeps the trigonal structure within space group $P\bar{3}m1$ with a reduction of the c/a ratio due to the departure of Li. This is especially visible for the fully de-lithiated compound resulting into "$2\square_{Li}ZrN_2$", where $\square_{Li}$ designates a lithium vacancy, characterized by a largely reduced c/a ratio of 1.28. The internal atomic positions are also modified but the major changes occur for the cell volume which is only slightly reduced upon the departure of one lithium but largely reduced by ~ 10 Å^3 for the departure of two lithium atoms and the reduction of the c/a ratio from 1.62 for "$\square_{Li}LiZrN_2$" down to 1.28 for "$2\square_{Li}ZrN_2$". Also it can be noted that the departure of one lithium leads to a shorter Li–N distance and a reduction of the Zr–N separation. This translates a stronger overall bonding in "$\square_{Li}LiZrN_2$".
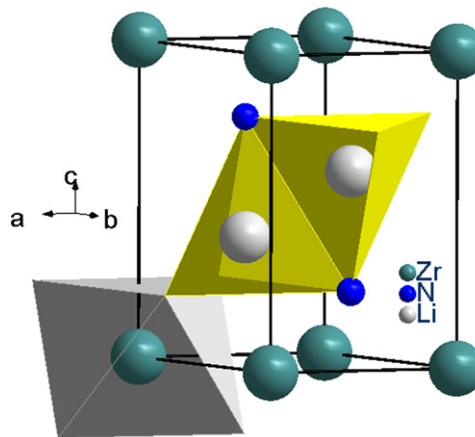
Fig. 1. The trigonal structure of Li_2ZrN_2. The edge-sharing LiN_4 tetrahedra and one ZrN_6 octahedron are emphasized.

Table 1
Li_2ZrN_2 and hypothetic Li de-intercalated phases. Experimental and calculated (italics) lattice parameters. Zr (1a) at (000).

$P\bar{3}m1$	Li_2ZrN_2, exp. [24]/calc.	"$\square_{Li}LiZrN_2$" calc.	Li-free Li_2ZrN_2 ($2\square_{Li}ZrN_2$) calc.
a (Å)	3.285/3.28	3.29	3.38
c (Å)	5.461/5.44	5.34	4.33
c/a	1.66/1.66	1.62	1.28
V (Å^3)	51.036/50.63	49.95	41.20
N (2d) (1/3 2/3 z)	z=0.223/0.228	z=0.207	z=0.23
Li (2d) (1/3 2/3 z')	z'=0.613/0.614	z'=0.417	z': –
Shortest distances (Å)	Li–N: 2.09/2.08	Li–N: 1.95	Li–N: –
	Zr–N: 2.25/2.26	Zr–N: 2.17	Zr–N: 2.19
Energy (eV)	–34.60	–30.22	–24.82
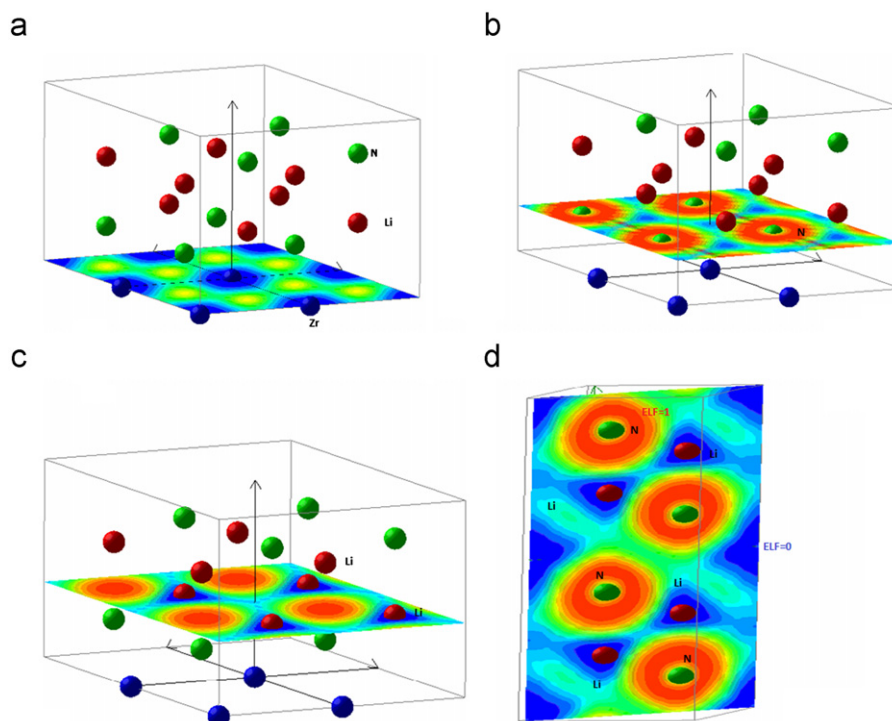
Fig. 2. Electron localization function ELF plots for Li_2ZrN_2 over 4 adjacent cells, showing (a) the basal plane at $z=0$ containing Zr, (b) the plane comprising N, (c) the plane containing Li, and (d) vertical plane with Li and N. Blue, green and red areas designate weak, free electron like and strong localizations respectively (see text). (For interpretation of the references to color in this figure legend, the reader is referred to the web version of this article).

These results would indicate less perturbation of the structure with one lithium equivalent departed and large changes when a second lithium equivalent is removed. The calculated total energies can be used to assess the free energy of the process. For this purpose we further calculate lithium metal with the same potentials and method to obtain a total energy per atom of -1.909 eV. Using the total energy values in Table 1, the Gibbs free energy change in the de-intercalation process of Li_2ZrN_2 is:

For the removal of one lithium equivalent:

$$\Delta G_1 = E(Li_2ZrN_2) - E(Li) - E(\square_{Li}LiZrN_2) = -2.47 \text{ eV}.$$

For the removal of a second lithium equivalent:

$$\Delta G_2 = E(\square_{Li}LiZrN_2) - E(Li) - E(2\square_{Li}ZrN_2) = -3.49 \text{ eV}.$$

Both ΔG_1 and ΔG_2 values are larger than the ones obtained for the binary silicide $Li_{15}Si_4$ ($\Delta G = -1.136$ eV [8]) and the ternary silicide YLiSi ($\Delta G = -1.69$ eV [16]). They correspond, with inverse sign, to the average de-intercalation voltage, V. It is interesting to note the 1.4 times larger magnitude for the removal of the second lithium equivalent, which is concomitant with a smaller Li–N distance, leading to a significant stabilization of the mono-delithiated compound. The de-intercalation voltage for the removal of one lithium equivalent, 2.47 V, is intermediate between the highest voltage magnitudes for the lithium intercalation compounds $LiTO_2$ ($T=3d$ transition metal) [39] with values amounting to $\sim$3–4 V and Li_xSi binaries such as $Li_{15}Si_4$ with $\sim$0.30 V [8]. Then Li_2ZrN_2 is found intermediate between oxide intercalation compounds and silicides [8,16].

In order to further assess these features, we analyze the charge density issued from the self consistent calculations using the AIM (atoms in molecules theory) approach [40] developed by Bader who devised an intuitive way of splitting molecules into atoms as based purely on the electronic charge density. Typically in chemical systems, the charge density reaches a minimum

between atoms and this is a natural region to separate atoms from each other. Such an analysis can be useful when trends between similar compounds are examined; they do not constitute a tool for evaluating absolute ionizations. The results of computed charge changes (ΔQ) are such that they lead to neutral compounds: Li_2ZrN_2: Li: $+1$; Zr: $+3.28$; N: -2.64, leading to an average charge transfer of ± 5.28 electrons; "$LiZrN_2$": Li: $+1$; Zr: $+3.33$; N: -2.16, leading to an average charge transfer of ± 4.34 electrons; and "ZrN_2": Zr $+3.4$; N: -1.7 with a charge transfer of ± 3.4 electrons.

These values should be compared with the formal ones assuming a full departure/gain of electrons in the valence states of the atomic constituents: Li ($2s^1$); Zr ($5s^2$, $4d^2$) and N ($2s^2$, $2p^3$). With the three compositions considered, this leads to 6, 5 and 4 electrons transfer. Despite their larger magnitudes versus Bader charges, the values follow the same trend of decrease along the series of studied compositions. Then Li_2ZrN_2 has a closed shell like configuration with all quantum states occupied as follows for the valence states: $2 \times$ Li ($2s^0$); $1 \times$ Zr ($5s^0$, $4d^0$) and $2 \times$ N($2s^2$, $2p^{3+3}$), i.e. with a departure of 6 electrons from Li/Zr and an occupation of all the six $2p$ states of the two nitrogen atoms. This is opposite to "$\square_{Li}LiZrN_2$" and "$2\square_{Li}ZrN_2$", respectively with one and two less electrons, which should present holes in the valence band with consequences on the electronic properties such as the metal/insulating character determined from the density of states (DOS)—vide infra. Thus the passage from Li_2ZrN_2 to hypothetic "$\square_{Li}LiZrN_2$" and then to "$2\square_{Li}ZrN_2$" signals the decrease of the ionic character (removal of Li) which is consequently largest for "$2\square_{Li}ZrN_2$". It needs to be mentioned here that "ZrN_2" itself does not exist; only N excess ZrN is known ($ZrN_{1.22}$) [23]. This would indicate a destabilization of the compound if more than one lithium equivalent is removed, as the calculations pointed out. Consequently partial delithiation leading to $Li_{2-x}ZrN_2$ ($x=\sim 1$) is favored.

Finally the electrons transfer from Li to N can be illustrated by the electron localization function ELF [41] obtained from real

space calculations: $ELF = (1 + \chi\sigma^2)^{-1}$. In this expression the ratio $\chi\sigma = D\sigma/D\sigma^0$ where $D\sigma = \tau\sigma - \nabla s - 1/4(\nabla\rho\sigma)^2/\rho\sigma$ and $D\sigma^0 = 3/5(6\pi^2)^{2/3}\rho\sigma^{5/3}$ correspond, respectively, to a measure of Pauli repulsion ($D\sigma$) of the actual system and to the free electron gas repulsion ($D\sigma^0$) and $\tau\sigma$ is the kinetic energy density. The ELF function is normalized between 0 (zero localization, blue areas) and 1 (strong localization, red areas) with the value of 1/2 corresponding to a free electron gas behavior (green areas). Fig. 2 shows the ELF contour plots for horizontal planes containing Zr (a), N (b), Li (c) and a vertical plane comprising Li and N. Whereas there is no electron localization around Zr (a) and Li (c, d) and green areas between them, there is a significant localization (orange-red areas) around N (b). This illustrates furthermore the charge density analysis above. The vertical plane along the c-axis (Fig. 2d) shows the layer-like structure of the compound with ~ 0 and ~ 1 ELF around Li and N, respectively.

5. Electronic structure and chemical bonding

Using the calculated lattice parameters in Table 1 we analyze the electronic structure and the chemical bonding using all electron calculations with the full potential ASW method. The site projected density of states (PDOS) for Li_2ZrN_2, "$\square_{Li}LiZrN_2$" and "$2\square_{Li}ZrN_2$" are shown in Fig. 3.

From the presence of a band gap of 1.8 eV at the top of the valence band (VB) E_V, the zero energy along the x-axis is considered with respect to E_V and Li_2ZrN_2 is a small gap insulator, in agreement with its light-green color [24]. This follows from the closed shell like electronic configuration discussed above along with Bader charges. The VB shows a large contribution from nitrogen due to twice as much N versus Zr in the structure and to the charge transfer from Li and Zr to N. Its s states are low lying at ~ -13 eV and the p states are found from -5 eV up to E_V. Those states mix with itinerant Zr d states within the VB; Zr being an early 4d element, its d band is centered within the empty conduction band (CB). Li PDOS resemble the valence states of Zr and N and quantum mixing is expected between them as it is illustrated in next section of chemical bonding. It is worth noting the dominating N p states at the top of the VB which differentiate the nitrides from the oxides whose VB top is dominated by the T states.

The removal of one equivalent of lithium leading to "$\square_{Li}LiZrN_2$" involves one electron less so that the top of the VB is rigidly shifted within the nitrogen states (creation of a hole) as it can be shown in Fig. 3b. The compound is now metallic and energy reference is with respect to the Fermi level (E_F). This feature is also observed for "$2\square_{Li}ZrN_2$" in Fig. 3c and a metallic like character is also observed. The decrease of the ionic character, as suggested from the Bader charges, is illustrated by a slightly broadened VB particularly for the s-like blocks, especially in the lithium-free hypothetic compound. The resemblance between the DOS in the three panels shows that lithium plays little role in the change of the structure which is mainly ensured by Zr and N binding. Similar changes in the electronic structure occur for the various intercalated phases of ZrN versus Li_xZrN and ZrNCl versus Li_xZrNCl. For details we refer to a recent overview [42].

This is further exhibited in Fig. 4 showing the COOP for the three compounds Li_2ZrN_2 (a) "$\square_{Li}LiZrN_2$" (b) and "$2\square_{Li}ZrN_2$" (c) accounting for atom multiplicities (Table 1). The whole range of the VB is of bonding character (positive COOP) for the main interaction, Zr–N as well as for Li–N. The Li–Zr bond is negligible as it can be expected from the electropositive nature of both and their large separation (~ 2.8 Å). The N–N interaction is of half bonding/half antibonding character so that the large N PDOS at the top of the VB is due to antibonding (repulsive) N–N states. Interestingly, the N–N antibonding character is of less magnitude
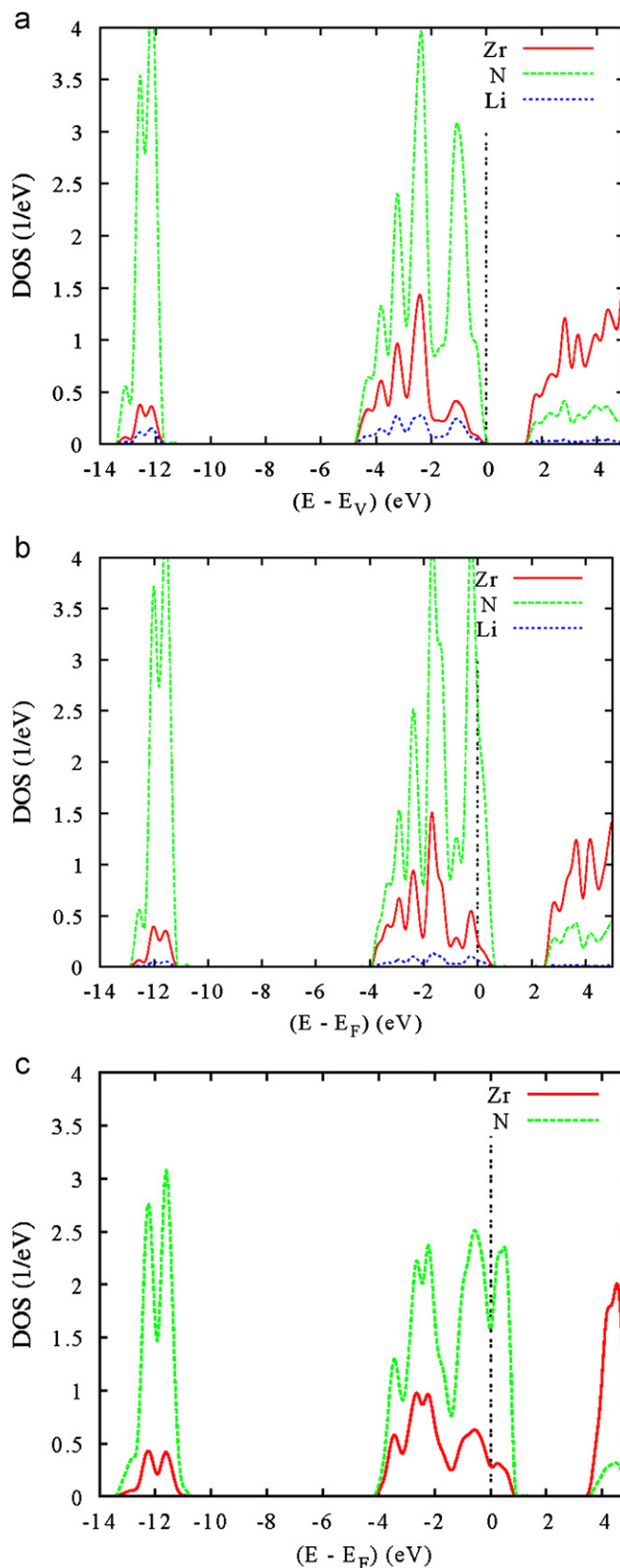
Fig. 3. Site projected density of states (PDOS) for Li_2ZrN_2 (a), $\square_{Li}LiZrN_2$ (b) and $2\square_{Li}ZrN_2$ (c) for all atom multiplicities.

from Li_2ZrN_2 (Fig. 4a) to "$\square_{Li}LiZrN_2$" (Fig. 4b) and "$2\square_{Li}ZrN_2$" (Fig. 4c) as the Fermi level is moved down within the VB (cf. DOS section). This is also concomitant with the larger binding energy
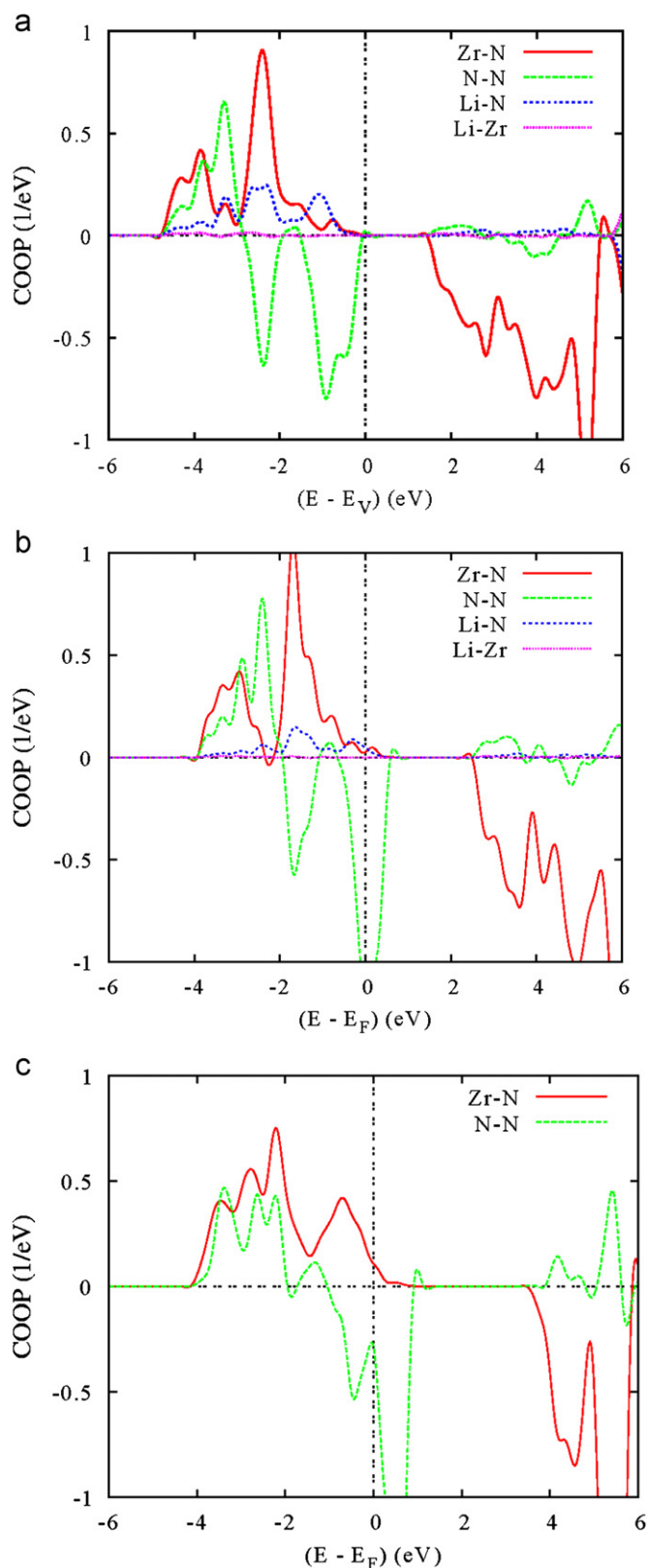
Fig. 4. Chemical bonding in Li_2ZrN_2 (a), "$\square_{Li}LiZrN_2$" (b) and "$2\square_{Li}LiZrN_2$" (c) for all atom multiplicities.

obtained from above energy differences calculated for Li_2ZrN_2 and "$\square_{Li}LiZrN_2$".

References

[1] M. Yoshio, R.J. Brodd, A. Kozawa (Eds.), Lithium-Ion Batteries: Science and Technologie, Springer, New York, 2009.
[2] K.E. Aifantis, S.A. Hackney, R.V. Kumar (Eds.), High Energy Density Lithium Batteries, Wiley-VCH, Weinheim, 2010.
[3] R.A. Huggins, Lithium Alloys Electrodes, in: D. Claus, J.O. Besenhard (Eds.), Handbook of Battery Materials, Wiley-VCH, Weinheim, 2011, pp. 405–432.
[4] R. Pöttgen, T. Dinges, H. Eckert, P. Sreeraj, H.-D. Wiemhöfer, Z. Phys. Chem. 224 (2010) 1475.
[5] V.S. Kolosnitsyn, E.V. Karaseva, Russ. J. Electrochem. 44 (2008) 506.
[6] J. Cabana, L. Monconduit, D. Larcher, M.R. Palacín, Adv. Mater. 22 (2010) E170.
[7] D.H. Gregory, Coord. Chem. Rev. 215 (2001) 301.
[8] Y. Kubota, M.C.S. Escaño, H. Nakanishi, H. Kasai, J. Appl. Phys. 102 (2007) 053704.
[9] A. Honda, S. Higai, N. Wada, Y. Sakabe, J. Phys. Chem. Solids 69 (2008) 1353.
[10] T. Dinges, U. Ch. Rodewald, S.F. Matar, H. Eckert, R. Pöttgen, Z. Anorg. Allg. Chem. 635 (2009) 1894.
[11] T. Dinges, R.-D. Hoffmann, L. van Wüllen, P. Henry, H. Eckert, R. Pöttgen, J. Solid State Electrochem. 15 (2011) 237.
[12] A. Kuhn, P. Sreeraj, R. Pöttgen, H.-D. Wiemhöfer, M. Wilkening, P. Heitjans, J. Am. Chem. Soc. 133 (2011) 11018.
[13] A. Kuhn, M. Wilkening, S. Puravankara, R. Pöttgen, H.-D. Wiemhöfer, P. Heitjans, Angew. Chem. 123 (2011) 12305.
[14] S. Dupke, T. Langer, R. Pöttgen, M. Winter, H. Eckert, Solid State NMR 40, in press. < http://dx.doi.org/10.1016/j.ssnmr.2011.09.002 > .
[15] T. Langer, S. Dupke, H. Eckert, S.F. Matar, M. Winter, R. Pöttgen, Solid State Sci. 14 (2012) 367.
[16] S.F. Matar, R. Pöttgen, N. Ouaini, Solid State Sci. 14 (2012) 375.
[17] R. Juza, Adv. Inorg. Radiochem. 9 (1966) 81.
[18] R. Juza, K. Langer, K. von Benda, Angew. Chem. 80 (1968) 373.
[19] N.E. Brese, M. O'Keeffe, Struct. Bonding 79 (1992) 307.
[20] R. Niewa, H. Jacobs, Chem. Rev. 96 (1996) 2053.
[21] R. Kniep, Pure Appl. Chem. 69 (1997) 185.
[22] R. Niewa, F.J. DiSalvo, Chem. Mater. 10 (1998) 2733.
[23] A.P. Palisaar, R. Juza, Z. Anorg. Allg. Chem. 384 (1971) 1.
[24] R. Niewa, H. Jacobs, Z. Kristallogr. 210 (1995) 513.
[25] O.V. Volkova, V.P. Obrosov, N.N. Batalov, Z.S. Martem'yanova, Elektrokhimiya 29 (1993) 1372.
[26] O.V. Zheltonozhko, V.P. Obrosov, N.N. Batalov, I.V. Korzun, in: Proceedings of the Electrochemical Society 93-9 on Molten Salt Chemistry and Technology, 1993, p. 578.
[27] P. Hohenberg, W. Kohn, Phys. Rev. 136 (1964) B864.
[28] W. Kohn, L.J. Sham, Phys. Rev. 140 (1965) A1133.
[29] G. Kresse, J. Furthmüller, Phys. Rev. B 54 (1996) 11169.
[30] G. Kresse, J. Joubert, Phys. Rev. B 59 (1999) 1758.
[31] P.E. Blöchl, Phys. Rev. B 50 (1994) 17953.
[32] J. Perdew, K. Burke, M. Ernzerhof, Phys. Rev. Lett. 77 (1996) 3865.
[33] W.H. Press, B.P. Flannery, S.A. Teukolsky, W.T. Vetterling, Numerical Recipes, Cambridge University Press, New York, 1986.
[34] M. Methfessel, A.T. Paxton, Phys. Rev. B 40 (1989) 3616.
[35] H.J. Monkhorst, J.D. Pack, Phys. Rev. B 13 (1976) 5188.
[36] A.R. Williams, J. Kübler, C.D. Gelatt, Phys. Rev. B 19 (1979) 6094.
[37] V. Eyert, The Augmented Spherical Wave Method—A Comprehensive Treatment, Lecture Notes in Physics, Springer, Heidelberg, 2007.
[38] R. Hoffmann, Angew. Chem. Int. Ed. Engl. 26 (1987) 846.
[39] M.K. Aydinol, A.F. Kohan, G. Ceder, K. Cho, J. Joannopoulos, Phys. Rev. B 56 (1997) 1354.
[40] R. Bader, Chem. Rev. 91 (1991) 893.
[41] A.D. Becke, K.E. Edgecombe, J. Chem. Phys. 92 (1990) 5397.
[42] C.M. Schurz, L. Shlyk, T. Schleid, R. Niewa, Z. Kristallogr. 226 (2011) 395.